Microporous and Mesoporous Materials 242 (2017) 256–263

Contents lists available at ScienceDirect

Microporous and Mesoporous Materials

journal homepage: www.elsevier.com/locate/micromeso

Keggin-Al_{30} pillared montmorillonite

Jianxi Zhu [a, *], Ke Wen [a, b], Ping Zhang [a, b], Yuebo Wang [c], Lingya Ma [a], Yunfei Xi [d, **], Runliang Zhu [a], Hongmei Liu [a], Hongping He [a]

[a] CAS Key Laboratory of Mineralogy and Metallogeny, Guangdong Provincial Key Laboratory of Mineral Physics and Materials, Guangzhou Institute of Geochemistry, Chinese Academy of Sciences, 511 Kehua Street, Guangzhou, 510640, China
[b] University of Chinese Academy of Sciences, Beijing, 100049, China
[c] Institute of Surface-Earth System Science, Tianjin University, 92 Weijin Road, Tianjin, 300072, China
[d] School of Chemistry, Physics and Mechanical Engineering, Science and Engineering Faculty, Queensland University of Technology, 2 George Street, Brisbane, QLD, 4000, Australia

ARTICLE INFO

Article history:
Received 22 December 2016
Received in revised form
23 January 2017
Accepted 27 January 2017
Available online 30 January 2017

Keywords:
Pillared interlayered clays (PILCs)
Intercalations
Keggin-Al_{30}
Microporous materials
NMR spectroscopy

ABSTRACT

Pillared interlayered clays (PILCs) draw intensive attention in the fields of chemistry and material sciences, owing to their strong surface acidity and large microporosity. These materials are superior selective heterogeneous catalysts and adsorbents. However, conventional hydroxy-aluminum pillared clays are based on Al_{13}, which cannot provide desirable properties due to its inherent limitation of size. Herein, a convenient method has been developed to prepare Al_{30} PILCs from montmorillonite (Mt) and a base-hydrolyzed solution of Al (III) chloride. To the best of our knowledge, this is the first time that porous pillared interlayered Mt with large Al_{30} pillars (2×1×1 nm) has been successfully prepared. This fundamental work may open up entirely new avenues for developing novel PILCs as heterogeneous catalysts and porous adsorbents.

1. Introduction

As a two-dimensional layered nanomaterial, pillared interlayered clays (PILCs) have attracted intensive scientific and industrial attentions in recent 40 years [1,2], since their first announcement (with polycations of Al_{13}) in 1979 [3,4]. Strong surface acidity and a large number of micropores extend the applicabilities of PILCs as catalyst supports and shape-selective adsorbents [5,6]. They have also found applications as molecular sieves, selective adsorbents, thermal insulators, and electrochemical and optical devices [7]. Generally, they are prepared by exchanging charge-compensating cations between the swellable clay minerals with larger polymeric hydroxyl metal cations [8,9]. By this process, the layered clay is transformed into a thermally stable micro- and/or mesoporous material that retains its layer structure [10,11].

Microporosity is one of the most significant characteristics of PILCs. Three factors affect the size and shape of PILCs pores: (i) the size and shape of intercalated pillars; (ii) the valence/charge of pillars; (iii) the layer charge of layered silicate hosts [12]. Due to the importance of particle sizes of pillars in PILCs [7], numerous researchers have been looking for ideal pillars for nearly four decades. Inorganic cations with large particle sizes as pillars were reported, including polycations of Al [13–19], Ti [20,21], Fe [22,23], or their a composites such as Al/Ce [24], Al/Fe [25], Al/Co [26], etc.. However, to our knowledge, few of these cations are big enough to bring attractive porosity. Though, aluminum pillaring agents are well understood, structures of many other metal polycations need identification and their hydrolysis behaviors require a comprehensive investigation [27,28].

Hydrolysis chemistry of aluminum and analytical techniques of characterization have been greatly developed in recent years [29]. Researchers found that larger polycation species can be formed upon additional titration with a hard base, with the Keggin-type structure [30]. A new polycation of aluminum Keggin-Al_{30} ($[Al_{30}O_8(OH)_{56}(H_2O)_{24}]^{18+}$, Fig. 1B) was detected in the hydrolysis solutions of aluminum. With a 'Gemini-Keggin' structure, Al_{30} is composed of two units of Al_{13} ($[Al_{13}O_4(OH)_{24}(H_2O)_{12}]^{7+}$, Fig. 1A),

* Corresponding author.
** Corresponding author.
E-mail addresses: zhujx@gig.ac.cn (J. Zhu), wenke@gig.ac.cn (K. Wen), zhangp@gig.ac.cn (P. Zhang), wangyuebo@tju.edu.cn (Y. Wang), malingya@gig.ac.cn (L. Ma), y.xi@qut.edu.au (Y. Xi), zhurl@gig.ac.cn (R. Zhu), hmliu@gig.ac.cn (H. Liu), hehp@gig.ac.cn (H. He).

http://dx.doi.org/10.1016/j.micromeso.2017.01.039
1387-1811/

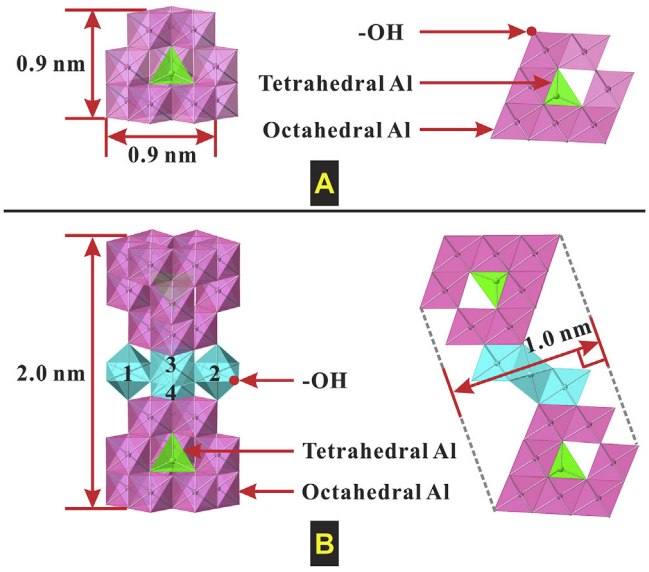

Fig. 1. Structural representation of (A) Al_{13} and (B) Al_{30} species.

linked by four octahedral aluminum monomers [31]. Compared with Al_{13}, Al_{30} has bigger particle size, higher ion charge density and more OH groups. Characterization of aluminum polycations containing Al_{13} and Al_{30} opens new avenue in the aqueous chemistry of aluminum [32]. Al_{30} cation has attracted a lot of attention [33–35], since its structure was revealed in 2000 [36].

Butman et al. made a good attempt to synthesize a "giant" pillared clay via a complicated hydrothermal process, however, no obvious enhancement in property was observed and key evidences were ambiguous [37]. The present work reports an effective method to prepare Al_{30} pillared interlayered montmorillonite (Al_{30}-PILM) and provides a theoretical guide for the development of novel porous adsorbents and catalytic materials.

2. Experimental

2.1. Materials

Calcium-montmorillonite (Mt) was obtained from Inner Mongolia, China. This sample has a very high purity above 95%, only a small amount of quartz was identified as the impurity by the powder X-ray diffraction (XRD) measurement. The main chemical composition (wt%) of Mt was investigated by X-ray fluorescence (XRF), and the results were reported in Table 1. Cation exchange capacity (CEC) of this Mt was determined by the adsorption quantity of $[Co(NH_3)_6]^{3+}$ [38,39], with a value at 110.5 mmol/100 g [11,14,40].

Aluminum chloride ($AlCl_3 \cdot 6H_2O$), sodium hydroxide (caustic soda, NaOH) and silver nitrate ($AgNO_3$) were purchased from Tianjin Fuchen chemical reagent factory. All chemicals are of analytical grade and used without further purification. Distilled water from an Ultra-pure Water Purifier was used.

2.2. Preparation of intercalating solutions

Al_{13} intercalating solution (Al_{13}-INTS): Similar to a procedure reported in literature [41], an Al_{13} intercalating solution was prepared by dropwise addition of a 0.6 M NaOH solution into a 1.0 M $AlCl_3$ solution at a rate of 1 mL/min, under vigorous stirring using a water bath at 60 °C to get a final $[OH^-]/[Al^{3+}]$ molar ratio of 2.4. The concentration of Al in the obtained solution is 0.2 M. Subsequently, the mixture was continuously stirred for another 12 h, and "aged" for 24 h at 60 °C.

Al_{30} intercalating solution (Al_{30}-INTS): Under constant stirring, a 0.6 M of NaOH solution was slowly added into a 1.0 M $AlCl_3$ solution at a rate of 1 mL/min using an oil bath at 95 °C to obtain a final molar ratio $[OH^-]/[Al^{3+}] = 2.4$. The resulting solution was stirred at 95 °C for another 12 h, and then a further "aging" at 95 °C was applied for a day.

Both Al_{13} and Al_{30} solutions are colorless transparent liquids without any deposit, even after stored at room temperature for one month. The pH values of both solutions are at 3.0–4.0. Total aluminum concentration (Al_T) is 0.2 mol/L for two solutions.

2.3. Synthesis of intercalated and pillared samples

The intercalation of Mt by Al_{13} and Al_{30} polycations was carried out through ion exchange reaction with an Al/clay mole ratio of 4.0 mmol/g. Under various stirring, Mt powder was dispersed into the intercalating solutions of Al_{13} at 60 °C and Al_{30} at 95 °C, respectively. Two suspensions were stirred continuously for 24 h and then aged for 24 h at 60 °C and 95 °C, respectively. After being cooled down to the room temperature, the products were separated by filtration and washed with distilled water until the supernatant solution was free of chloride as indicated by $AgNO_3$ solution. The solid products were freeze-dried for 48 h, and denoted as Al_{13}-INTM and Al_{30}-INTM, respectively.

Al_{13} pillared interlayered Mt (Al_{13}-PILM) and Al_{30} pillared interlayered Mt (Al_{30}-PILM) samples were obtained after calcination of the intercalated products at 300 °C for 2 h.

2.4. Characterization methods

2.4.1. Liquid ^{27}Al NMR spectroscopy

^{27}Al NMR spectra were generated at 70 °C on a Fast Fourier Transformation spectrometer (JNM-ECA600, JOEL) in Tsinghua University, China. Samples were placed in a 5 mm NMR tube, and D_2O was injected into the center. The measurement was operated under the following condition: field strength of 14.09 T, single pulse method, resonating frequency at 156.39 MHz, X-acq-duration of 0.21 s, repetition time of 0.51 s, relaxation delay of 0.3 s and 2048 scans.

2.4.2. Solid-state ^{27}Al MAS NMR spectroscopy

Solid-state ^{27}Al MAS NMR experiments were carried out on a Bruker AVANCE III 600 spectrometer at a resonance frequency of 156.4 MHZ. ^{27}Al MAS spectra were recorded by the small-flip angle technique with a pulse length of 0.68 μs($<\pi/12$) and a 1s recycle delay. A 3.2 mm HX double-resonance MAS probe was used at a

Table 1
The main chemical composition of samples (wt%).

Samples	Al_2O_3	CaO	TFe_2O_3	K_2O	MgO	Na_2O	P_2O_5	SiO_2	TiO_2	LOI
Mt	15.93	2.42	5.25	0.09	4.72	0.65	0.31	59.28	0.27	9.63
Al_{13}-PILM	24.13	0.03	4.37	0.08	3.80	0.01	0.01	52.37	0.23	13.71
Al_{30}-PILM	28.35	0.02	4.06	0.04	3.31	0.06	0.20	47.54	0.21	15.11

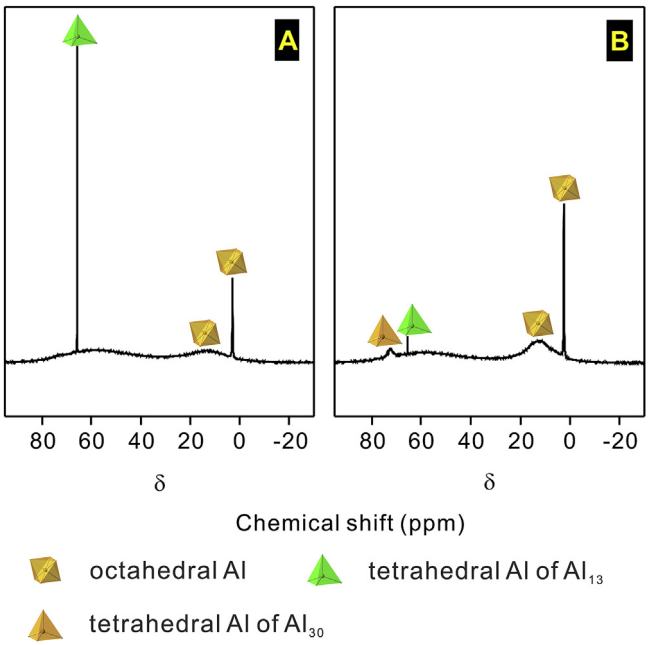

Fig. 2. Liquid ^{27}Al NMR spectra of (A) Al_{13} and (B) Al_{30} solutions which were synthesized at 60 °C and 95 °C, respectively. Al_T = 0.2 mol L^{-1}, molar ratio $[OH^-]/[Al^{3+}]$ = 2.4.

sample spinning rate of 15 kHz. The chemical shifts of ^{27}Al was referenced using a 1 mol L^{-1} aqueous $Al(NO_3)_3$ solution.

2.4.3. X-ray diffraction patterns

Powder X-ray diffraction (XRD) patterns were collected using Ni-filtered Cu Kα radiation (λ = 0.154 nm) on a Bruker D8 Advance diffractometer, which was operated at 40 kv and 40 mA with a scan rate of 1°(2θ)/min between 3° and 60°. Basal spacing were determined from the 2θ values of the corresponding basal reflections.

2.4.4. Transmission electron micrographs

Transmission electron microscopy (TEM) images were collected on a FEI Talos F200s transmission electron microscope operating at an accelerating voltage of 200 kV. For TEM observation, samples were ultrasonically dispersed in ethanol (100 mg/L) for 5 min. Sample suspensions were dropped onto carbon-coated copper grids and left to dry for 10 min.

2.4.5. N_2 adsorption-desorption isotherms

Nitrogen adsorption-desorption isotherms were determined at liquid nitrogen temperature (−196 °C) with a gas sorption analyzer (Micromeritics ASAP 2020 instrument). Samples were degased at 120 °C for 12 h before tests. The specific surface area (SSA) was calculated by the Brunauer-Emmett-Teller (BET) method [42]. Total pore volume was evaluated from nitrogen uptake at a relative pressure of 0.99 [43]. Microporous specific surface area and micropore volume were calculated using the t-method [44]. The pore size distribution (PSD) analysis were carried out by the nonlocal density functional theory (NLDFT) for pillared clay [45], which is more appropriate for evaluating a bi-dimension porous structure [46].

3. Results and discussion

3.1. Liquid ^{27}Al NMR analysis

In Fig. 2A, the resonance peak at δ = 3.0 ppm is assigned to the Al monomer (Al_m), namely the symmetric hexa-aquoaluminium

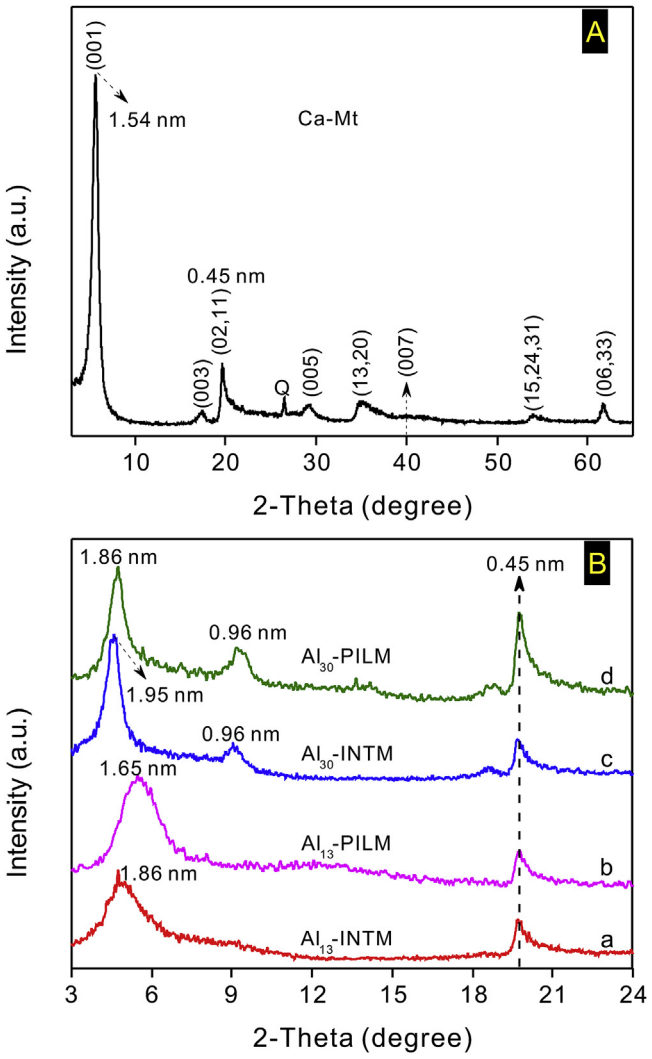

Fig. 3. Powder X-ray diffraction patterns of (A) Mt and (B) intercalated and pillared Mt samples; Q, quartz.

$[Al(H_2O)_6]^{3+}$ [47]. The sharp resonance peak at δ = 65.7 ppm corresponds to the central tetrahedral aluminum (AlO_4) in Al_{13} [48]. The broad peak at δ = 12.8 ppm is attributed to the octahedral aluminum of external Keggin shells in Al_{13}. Located in an asymmetric coordination environment, the extremely fast spin relaxation of octahedral aluminum shortens the relaxation time and broadens the line width [49,50]. In Fig. 2B, similar to the spectrum of Al_{13} solution, three resonance peaks at δ = 2.6 ppm, 65.3 ppm and 12.1 ppm were detected, respectively. Sharp peaks at δ = 2.6 ppm and δ = 65.3 ppm are assigned to the Al monomer and the central tetrahedral aluminum in Al_{13}, respectively. The broad peak at δ = 12.1 ppm is attributed to the external octahedral aluminum [48]. A new resonance peak at δ = 72.5 ppm (Fig. 2B) was detected. This peak corresponds to the central tetrahedral aluminum in Al_{30} [48], indicating the successful synthesis of Al_{30}.

Although both Al_{13} and Al_{30} species are kinetic intermediate products in the process of aluminum hydrolysis and polymerization, Al_{30} is more stable than Al_{13} [32]. It is because two Al_{13} Keggin units are connected by a crown made of four hexa-coordinated aluminum (AlO_6) ("1" to "4" in Fig. 1B) in Al_{30}. The dislocation of two Keggin units on the crystal structure of Al_{30} (the schematic on the right in Fig. 1B) causes an overall reduction of the structure symmetry. Therefore, the typical resonance peak has shifted from

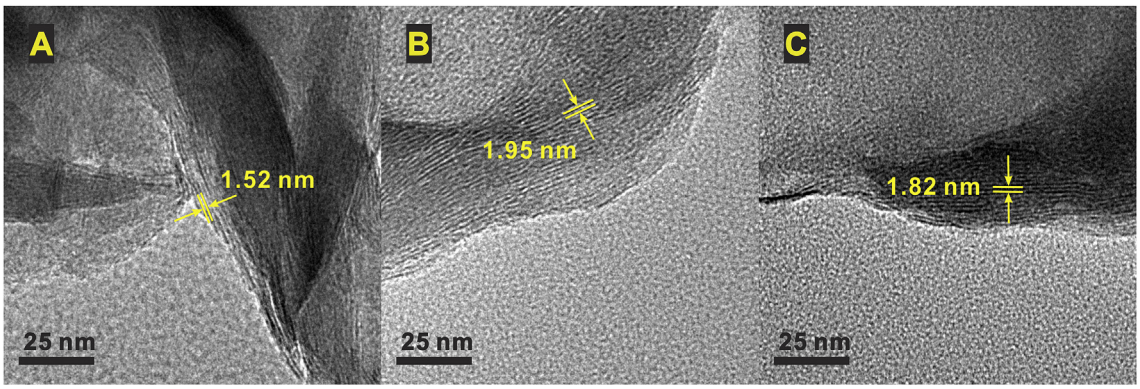

Fig. 4. TEM images of (A) Mt, (B) Al_{30}-INTM, (C) Al_{13}-INTM.

65.7 ppm to 72.5 ppm, which indicates that the Al_{30} intercalating agent has been successfully prepared.

3.2. X-ray diffraction (XRD)

In Fig. 3, an intense reflection at $2\theta = 5.7°$ ($d = 1.54$ nm) corresponds to the (001) basal reflection of Mt. Since the thickness of an individual layer of Mt is 0.96 nm, the interlayer space is about 0.58 nm. After intercalation with Al_{13} cations, the d_{001} value of Al_{13} interlayered Mt (Al_{13}-INTM) increases to 1.86 nm (Fig. 3Ba), which corresponds to an interlayer separation of 0.9 nm. This value is in accordance with the average diameter of Keggin-like Al_{13} cation particle (0.9 nm), indicating a successful intercalation of Al_{13} into Mt [51]. After calcination at 300 °C, the d_{001} value of Al_{13}-PILM (Fig. 3Bb) decreases to 1.65 nm. The interlayer separation of Al_{30} interlayered Mt (Al_{30}-INTM, 1.0 nm) is 0.1 nm larger than that of Al_{13}-INTM (0.9 nm), with a d_{001} value at 1.95 nm (Fig. 3Bc). After calcination, the d_{001} value of obtained Al_{30}-PILM decreases to 1.86 nm, which is 0.2 nm larger than that of Al_{13}-PILM. It was caused by the removal of water molecules associated with interparticles and interlayer surfaces, and the dehydroxylation of interlayer Al_{30} cations and Mt layers [52]. Broad reflections at about 9° 2θ (d = 0.96 nm) were detected in XRD patterns of both Al_{30}-INTM and Al_{30}-PILM, corresponding to the thickness of an individual Mt layer (Fig. 8B). The reflection at 0.96 nm in both Al_{30}-INTM and Al_{30}-PILM may be attributed to a highly interstratified structure created by large number of Al_{30} particles (Fig. 8B).

As mentioned above, an Al_{30} cation consists of two units of Keggin-Al_{13}, with a linkage of four octahedral aluminum monomers (AlO_6, denoted as "1", "2", "3", "4" in Fig. 1B, respectively). However, different orientations of these Al_{13} units give rise to a slight increment in diameter for the Al_{30} cation than the Al_{13} cation, which leads to a 0.1 nm larger expansion for the Mt layers and is likely to bring enhanced microporosity on the resultant material.

3.3. Morphological properties

In Fig. 4, different samples show a similar morphology, with the clay platelets stacked in an orderly manner. Mt has a d_{001} value of approximately 1.52 nm (Fig. 4A). With the intercalation of Keggin-

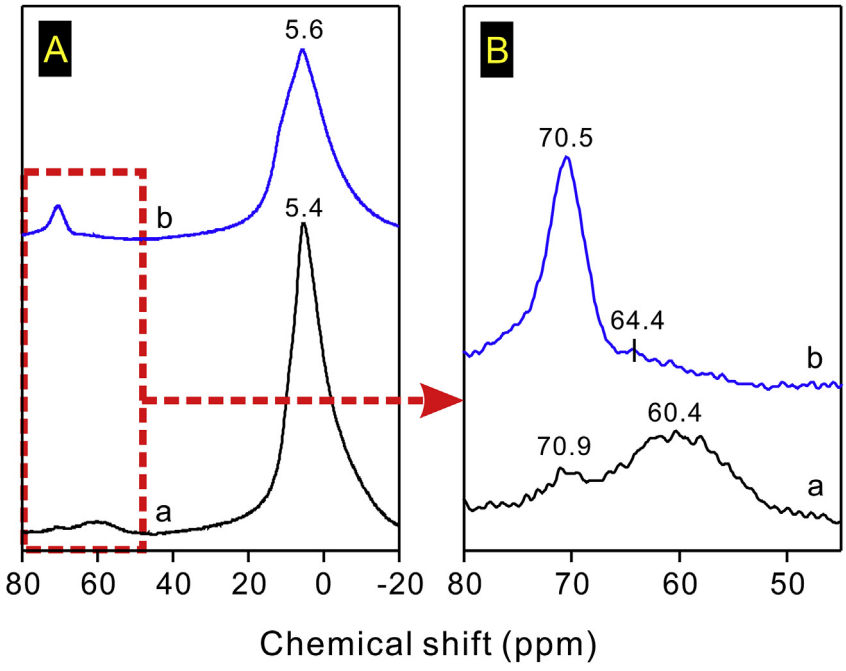

Fig. 5. Solid-state ^{27}Al MAS NMR spectrum of (a) Mt and (b) Al_{30}-INTM.

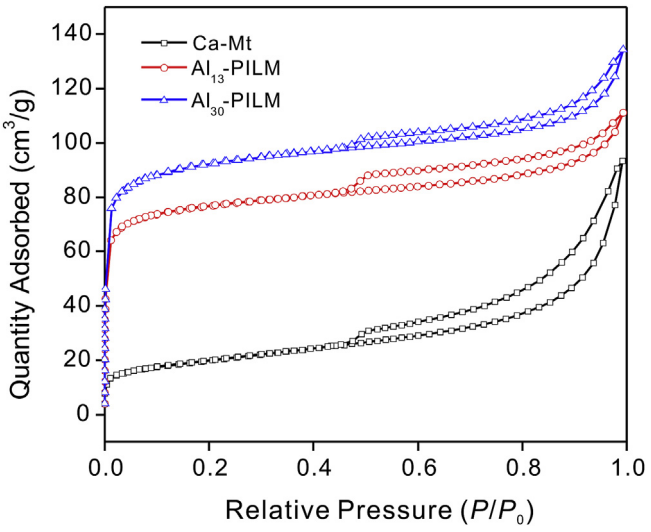

Fig. 6. Nitrogen adsorption-desorption isotherms of Mt and pillared samples.

Al_{13} cations, the basal spacing of Al_{13} intercalated Mt (Al_{13}-INTM) increases to 1.82 nm (Fig. 4C). Compared to Al_{13}-INTM, Al_{30} intercalated Mt (Al_{30}-INTM) shows an expanded interlayer space at 1.95 nm (Fig. 4B). These results are well consistent with the XRD analyses. Results from XRD and TEM strongly support that the large d_{001} values are resulted from the intercalation of polyaluminum particles into the host Mt layers. TEM images also indicate the existence of a highly porous structure in the pillared interlayered Mt. It should be noticed that the intercalated samples are probably not stable during the TEM observation. The high temperature generated from the electron beam might cause the transformation of intercalated particles into pillared ones.

3.4. Solid-state ^{27}Al MAS NMR analysis

A strong and sharp signal at 5.4 ppm was detected in the range of -20–20 ppm (Fig. 5 Aa) and assigned to the mono Al in the octahedral sheet of Mt [53]. Two broad peaks at 60.4 ppm and 70.9 ppm (Fig. 5Ba), respectively, indicate the presence of tetrahedral Al [54,55]. These two peaks arise from the substitution of Al^{3+} for Si^{4+} in tetrahedral sheets [56]. In Fig. 5Ab, the signal at 5.6 ppm is attributed to the octahedral Al in layers of Mt and external shells of Al_{30} cation. Asymmetry of octahedral Al in the shell of Al_{30} make the peak wider than that of Mt (5.4 ppm). With the intercalation of Al_{30} cations, the signal of quadridentate Al in Mt tetrahedral sheets shifts from 60.4 ppm to 64.4 ppm (Fig. 5B). This is due to the interaction between Al_{30} cations and the charged layers of Mt. A small amount of Al_{13} cations may exist in the interlayer space of Al_{30}-INTM, because a signal of typical tetrahedral Al in Al_{13} of Al_{13}-PILM can be observed at near 64 ppm [53]. The isotropic chemical shift at 70.5 ppm (Fig. 5Bb) belongs to quadridentate Al of Al_{30} cations in Al_{30}-INTM [33], which is in good agreement with values for crystalline Al_{30} sulfate [32,57]. This intense resonance peak of Al_{30}-INTM (70.5 ppm) is quite different from that of Al_{13} (64 ppm) [53], due to the symmetric differences of their structures. Therefore, the existence of Al_{30} in Al_{30}-PILM can be confirmed. On the basis of XRD and TEM results, it is definite that Al_{30}-PILM has been synthesized successfully.

3.5. Main chemical composition

XRF datum of Mt, Al_{13}-PILM, Al_{30}-PILM are displayed in Table 1. On the basis of these results, we found that $(Al_2O_3)/(SiO_2)$ ratio values of samples was increased, with pillaring by polycations of Al_{13} and Al_{30}. The ratio values of $(Al_2O_3)/(SiO_2)$ for Mt, Al_{13}-PILM, and Al_{30}-PILM are 0.27, 0.46, and 0.60, respectively. Increment of aluminum was caused by the pillared polycations of aluminum, and the quantities of increased Al_2O_3 between

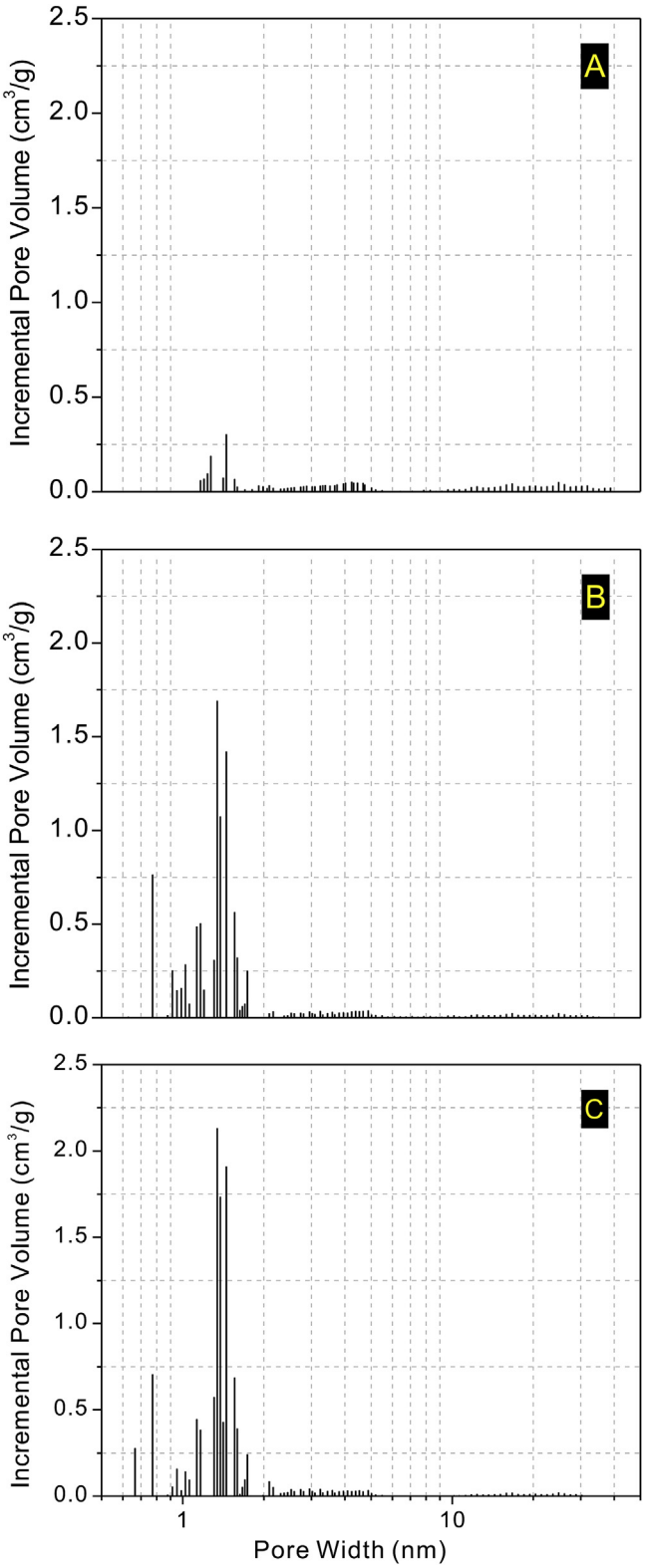

Fig. 7. Pore size distributioin patterns of (A) Mt, (B) Al_{13}-PILM and (C) Al_{30}-PILM.

Table 2
Structural parameters of the initial Mt, Al_{13}-PILM and Al_{30}-PILM samples.

Sample	SSA (m^2/g)[a]	S_{ext} (S_{micro}) (m^2/g)[b]	V_P (cm^3/g)[c]	$V_{\mu P}$ (V_{mP}) (cm^3/g)[d]	APD (nm)[e]
Mt	69.5	69.5 (0)	0.119	0 (0.119)	6.9
Al_{13}-PILM	258.8	135.6 (123.2)	0.161	0.051 (0.110)	2.4
Al_{30}-PILM	311.2	176.8 (134.4)	0.192	0.055 (0.137)	2.4

[a] SSA = total specific surface area (degas at 120 °C).
[b] S_{ext} = external surface area, evaluated from t-plot method; surface area of micropore (S_{micro}) is obtained by subtracting S_{ext} from total surface area (SSA).
[c] V_P = total porous volume, from the amount adsorbed at the relative pressure of 0.978.
[d] $V_{\mu P}$ = microporous volume, calculated by t-plot method; mesoporous volume (V_{mP}) = V_P -$V_{\mu P}$.
[e] APD = average pore diameter.

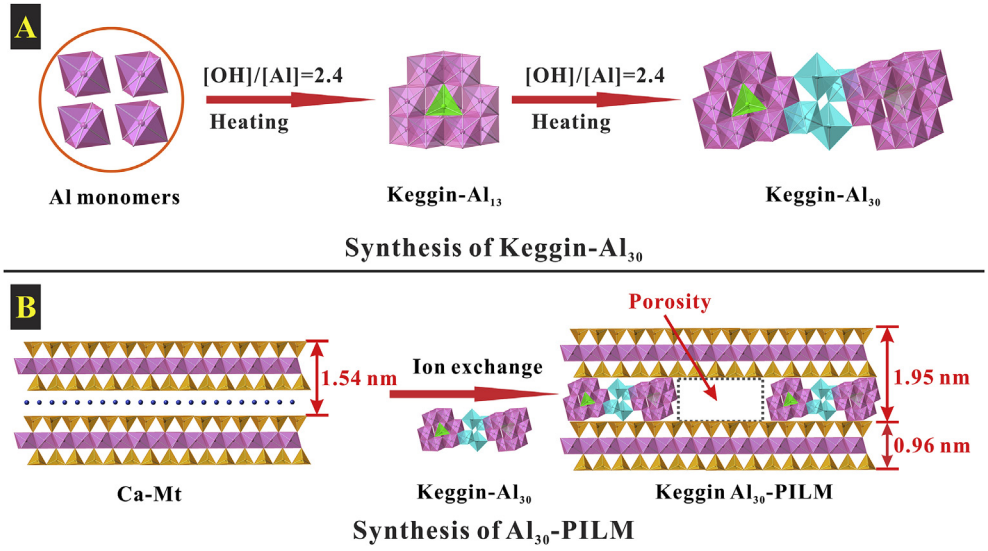

Fig. 8. Schematic representation of Al_{30}-PILM formation; two adjacent Al_{30} particles can exfoliate Mt layers and create a larger cavity.

montmorillonite layers in Al_{30}-PILM is nearly twice that of Al_{13}-PILM. By an approximate calculation, we found that Al_{30}-PILM contained about 0.12 mmol Keggin-Al_{30} polycations per gram, while Al_{13}-PILM contained about 0.17 mmol Keggin-Al_{13} polycations per gram.

3.6. Specific surface area and porosity

In Fig. 6, curves of Al_{13}-PILM and Al_{30}-PILM are distinctly different to that of Mt. After intercalation and calcination, both the N_2 adsorption-desorption isotherm types of Al_{13}-PILM and Al_{30}-PILM turned to type IV (IUPAC classification) [58], indicating a greater microporosity. In the region of relatively low pressure, both adsorption isotherms of the two pillared samples exhibit Langmuir adsorption type I, suggesting the presence of micropores. According to the quantities of N_2 adsorbed at very low relative pressure, Al_{30}-PILM has a larger micropore volume than Al_{13}-PILM. The hysteresis loops of the isotherms of pillared products may be caused by the three-dimensional co-aggregation of montmorillonite layers.

In Fig. 7, the pore size distributions of Mt, Al_{13} pillared interlayered Mt (Al_{13}-PILM) and Al_{30} pillared interlayered Mt (Al_{30}-PILM) show that the size of pores in these samples is quite non-uniform. Compared with the original Mt, the pillared samples of Al_{13} or Al_{30} possess fantastic porosity with pore diameters at about 1–2 nm. The enhanced porosities of Al_{13} or Al_{30} are resulted from the pillaring with inorganic cations, Keggin-Al_{13} and Al_{30}. The micropores dominate the major pore size distributions due to the permanent expansion of basal spaces, indicating the microporous feature of Keggin polycations pillared clay minerals. Meanwhile, incremental pore volumes of Al_{30}-PILM samples are larger than those of Al_{13}-PILM samples, and the former samples have a slight increase in pore width.

As summarized in Table 2, the pillaring process with inorganic polycations of Al_{13} and Al_{30} leads to a dramatic increment in SSA and porosity, because the polymerized Al cations have entered into interlayer space and pillared the Mt layers. Both microporosity and mesoporosity contribute to the total porosity and SSA in the resultant Al-PILMs, particularly to the micropores. The SSA and porosity of Al_{30}-PILM are much larger than those of Al_{13}-PILM. The larger textural parameters of Al_{30}-PILM are probably due to a larger cation size and higher ion charge of Al_{30}.

4. Conclusions

In conclusion, the method of hydrolysis of $AlCl_3$ with NaOH has been applied to prepare Al_{30}-PILM. High-field liquid ^{27}Al NMR results have proved that Al_{30} cations are main components in the intercalating solution, solid-state ^{27}Al NMR analysis of the intercalated products have confirmed that Al_{30} still exists. The combination of XRD and TEM have revealed the expansion of Mt layers, indicating the successful synthesis of Al_{30}-PILM. The porous structure of resultant product is from the expansion of Mt layers by Al_{30} cations. Compared with the structural parameters of Al_{13}-PILM, the big size of Al_{30} cation leads to a greater SSA (311.2 m^2/g) and V_p (0.192 cm^3/g) of Al_{30}-PILM. The possible schematic representation of Al_{30}-PILM synthesis is shown in Fig. 8.

Since Al_{30} has a relatively large particle size, high cation charges, and abundant hydroxyl groups, the intercalation of Al_{30} into montmorillonite may lead to more Lewis acid sites. Also, the thermal stability of Mt may be enhanced greatly. A further breakthrough will focus on optimization of synthesis condition, which may change the orientation of Al_{30} pillars from horizontal to vertical. The prospective configuration will definitely bring even larger interlayer spacing and microporosity. Overall, the fundamental work in this study is critical to the development of superior catalysts and adsorbent materials.

Acknowledgements

This work was supported by CAS/SAFEA International Partnership Program for Creative Research Teams (Grants 20140491534) and National Natural Science Foundation of China (Grant No. 41272060, 41502031, 41572031). This is a contribution No. IS-2340 from GIGCAS.

References

[1] W. Ye, B. Zhao, H. Gao, J. Huang, X. Zhang, Preparation of highly efficient and stable Fe, Zn, Al-pillared montmorillonite as heterogeneous catalyst for catalytic wet peroxide oxidation of Orange II, J. Porous Mater. 23 (2016) 301–310.
[2] L. Ma, J. Zhu, Y. Xi, R. Zhu, H. He, X. Liang, G.A. Ayoko, Simultaneous adsorption of Cd(II) and phosphate on Al_{13}pillared montmorillonite, RSC Adv. 5 (2015) 77227–77234.
[3] A. Gil, L.M. Gandia, M.A. Vicente, Recent advances in the synthesis and catalytic applications of pillared clays, Catal. Rev. 42 (2000) 145–212.
[4] D.E.W. Vaughan, R.J. Lussier, J.S.M. Jr, Pillared interlayered clay materials useful as catalysts and sorbents, Google Patents 1979.
[5] P. Yuan, X. Yin, H. He, D. Yang, L. Wang, J. Zhu, Investigation, on the delaminated-pillared structure of TiO_2-PILC synthesized by $TiCl_4$ hydrolysis method, Microporous Mesoporous Mater. 93 (2006) 240–247.
[6] A. Aznarez, R. Delaigle, P. Eloy, E.M. Gaigneaux, S.A. Korili, A. Gil, Catalysts based on pillared clays for the oxidation of chlorobenzene, Catal. Today 246 (2015) 15–27.
[7] M.A. Vicentea, A. Gilb, F. Bergaya, Pillared clays and clay minerals, in: F. Bergaya, G. Lagaly (Eds.), Handbook of Clay Science, second ed., Elsevier, 2013, pp. 523–557.
[8] L. Ma, J. Zhu, H. He, Q. Tao, R. Zhu, W. Shen, B.K.G. Theng, Al_{13}-pillared montmorillonite modified by cationic and zwitterionic surfactants: a comparative study, Appl. Clay Sci. 101 (2014) 327–334.
[9] F. Kooli, Porous clay heterostructures (PCHs) from Al_{13}-intercalated and Al_{13}-pillared montmorillonites: properties and heptane hydro-isomerization catalytic activity, Microporous Mesoporous Mater. 184 (2014) 184–192.
[10] R.A. Schoonheydt, T. Pinnavaia, G. Lagaly, N. Gangas, Pillared clays and pillared layered solids, Pure Appl. Chem. 71 (1999).
[11] Y. Wang, P. Zhang, K. Wen, X. Su, J. Zhu, H. He, A new insight into the compositional and structural control of porous clay heterostructures from the perspective of NMR and TEM, Microporous Mesoporous Mater. 224 (2016) 285–293.
[12] M.M. Herling, J. Breu, The largely unknown class of microporous hybrid materials: clays pillared by molecules, Z. für Anorg. Allg. Chem. 640 (2014) 547–560.
[13] Z. Qin, P. Yuan, S. Yang, D. Liu, H. He, J. Zhu, Silylation of Al_{13}-intercalated montmorillonite with trimethylchlorosilane and their adsorption for orange II, Appl. Clay Sci. 99 (2014) 229–236.
[14] Y. Wang, X. Su, X. Lin, P. Zhang, K. Wen, J. Zhu, H. He, The non-micellar template model for porous clay heterostructures: a perspective from the layer charge of base clay, Appl. Clay Sci. 116–117 (2015) 102–110.
[15] Y. Gao, W. Li, H. Sun, Z. Zheng, X. Cui, H. Wang, F. Meng, A facile in situ pillaring method—the synthesis of Al-pillared montmorillonite, Appl. Clay Sci. 88–89 (2014) 228–232.
[16] M. Pichowicz, R. Mokaya, Stability of pillared Clays: effect of compaction on the physicochemical properties of Al-Pillared clays, Chem. Mater. 16 (2003) 263–269.
[17] A. Aouad, A. Pineau, D. Tchoubar, F. Bergaya, Al-pillared montmorillonite obtained in concentrated media. Effect of the anions (nitrate, suflate and chloride) associated with the Al species, Clays Clay Miner. 54 (2006) 626–637.
[18] M.L. Occelli, A. Auroux, G.J. Ray, Physicochemical characterization of a Texas montmorillonite pillared with polyoxocations of aluminum. II. NMR and microcalorimetry results, Microporous Mesoporous Mater. 39 (2000) 43–56.
[19] M.L. Occelli, J.A. Bertrand, S.A.C. Gould, J.M. Dominguez, Physicochemical characterization of a Texas montmorillonite pillared with polyoxocations of aluminum Part I: the microporous structure, Microporous Mesoporous Mater. 34 (2000) 195–206.
[20] P. Yuan, X. Yin, H. He, D. Yang, L. Wang, J. Zhu, Investigation on the delaminated-pillared structure of TiO_2-PILC synthesized by $TiCl_4$ hydrolysis method, Microporous Mesoporous Mater. 93 (2006) 240–247.
[21] D. Chen, Q. Zhu, F. Zhou, X. Deng, F. Li, Synthesis and photocatalytic performances of the TiO_2 pillared montmorillonite, J. Hazard. Mater. 235–236 (2012) 186–193.
[22] P. Yuan, F. Annabi-Bergaya, Q. Tao, M. Fan, Z. Liu, J. Zhu, H. He, T. Chen, A combined study by XRD, FTIR, TG and HRTEM on the structure of delaminated Fe-intercalated/pillared clay, J. Colloid Interface Sci. 324 (2008) 142–149.
[23] L. Ma, Y. Xi, H. He, G.A. Ayoko, R. Zhu, J. Zhu, Efficiency of Fe–montmorillonite on the removal of Rhodamine B and hexavalent chromium from aqueous solution, Appl. Clay Sci. 120 (2016) 9–15.
[24] S. Zuo, Q. Huang, R. Zhou, Al/Ce pillared clays with high surface area and large pore: synthesis, characterization and supported palladium catalysts for deep oxidation of benzene, Catal. Today 139 (2008) 88–93.
[25] S.T. Khankhasaeva, D.V. Dambueva, E.T. Dashinamzhilova, A. Gil, M.A. Vicente, M.N. Timofeeva, Fenton degradation of sulfanilamide in the presence of Al,Fe-pillared clay: catalytic behavior and identification of the intermediates, J. Hazard. Mater. 293 (2015) 21–29.
[26] F. Bertella, S.B.C. Pergher, Pillaring of bentonite clay with Al and Co, Microporous Mesoporous Mater. 201 (2015) 116–123.
[27] M.B.d. Carvalho, J. Pires, A.P. Carvalho, Characterisation of clays and aluminium pillared clays by adsorption of probe molecules, Microporous Mater. (1996) 13.
[28] M.A. Vicente, A. Gil, F. Bergaya, Pillared clays and clay minerals, in: F. Bergaya, G. Lagaly (Eds.), Handbook of Clay Science, second ed., Elsevier, 2013, p. 35.
[29] S. Abeysinghe, D.K. Unruh, T.Z. Forbes, Surface modification of Al_{30} Keggin-type polyaluminum molecular clusters, Inorg. Chem. 52 (2013) 5991–5999.
[30] W.H. Casey, Large aqueous aluminum hydroxide molecules, Chem. Rev. 106 (2006) 1–16.
[31] Z. Wu, X. Zhang, C. Zhou, J. Pang, P. Zhang, A comparative study on the characteristics and coagulation mechanism of PAC-Al_{13} and PAC-Al_{30}, RSC Adv. (2016) 108369–108374.
[32] L. Allouche, F. Taulelle, Conversion of Al_{13} Keggin ε into Al_{30} a reaction controlled by aluminum monomers, Inorg. Chem. Commun. 6 (2003) 1167–1170.
[33] B.L. Phillips, J.S. Vaughn, S. Smart, L. Pan, Characterization of Al_{30} in commercial poly-aluminum chlorohydrate by solid-state Al ^{27}NMR spectroscopy, J. Colloid Interface Sci. 476 (2016) 230–239.
[34] K.W. Corum, S.E. Mason, Using density functional theory to study shape-reactivity relationships in Keggin Al-nanoclusters, Water Res. 102 (2016) 413–420.
[35] K.W. Corum, M. Fairley, D.K. Unruh, M.K. Payne, T.Z. Forbes, S.E. Mason, Characterization of phosphate and arsenate adsorption onto Keggin-type Al_{30} cations by experimental and theoretical methods, Inorg. Chem. 54 (2015) 8367–8374.
[36] J. Rowsell, L.F. Nazar, Speciation and thermal transformation in alumina sols: structures of the polyhydroxyoxoaluminum cluster $[Al_{30}O_8(OH)_{56}(H_2O)_{26}]^{18+}$ and its δ-Keggin Moieté, J. Am. Chem. Soc. 122 (2000) 3777–3778.
[37] M.F. Butman, A.G. Belozerov, N.S. Karasev, N.E. Kochkina, I.A. Khodov, N.L. Ovchinnikov, Structural and textural properties of pillared montmorillonite at intercalation of large Al- and Al/Ce-polyhydroxocomplexes, Nanotechnol. Russ. 10 (2015) 706–712.
[38] X. Hu, G. Lv, Y. Yang, Determination of cation-exchange capacity in clay $[Co(NH_3)_6]^{3+}$ exchange method, Chin. J. Anal. Chem. 28 (2000) 1402–1405.
[39] L. Zhu, R. Zhu, L. Xu, X. Ruan, Influence of clay charge densities and surfactant loading amount on the microstructure of CTMA–montmorillonite hybrids, Colloids Surf. A Physicochem. Eng. Asp. 304 (2007) 41–48.
[40] Y. Wang, X. Lin, K. Wen, J. Zhu, H. He, Effects of organic templates on the structural properties of porous clay heterostructures: a non-micellar template model for porous structure, J. Porous Mater. 22 (2014) 219–228.
[41] S. Zuo, R. Zhou, Influence of synthesis condition on pore structure of Al pillared clays and supported Pd catalysts for deep oxidation of benzene, Microporous Mesoporous Mater. 113 (2008) 472–480.
[42] D. Zhao, Q. Huo, J. Feng, B.F. Chmelka, G.D. Stucky, Nonionic triblock and star diblock copolymer and oligomeric surfactant syntheses of highly ordered, hydrothermally stable, mesoporous silica structures, J. Am. Chem. Soc. 120 (1998) 6024–6036.
[43] S.J. Gregg, K.S.W. Sing, H.W. Salzberg, Adsorption surface area and porosity, J. Electrochem. Soc. 114 (1967), 279C.
[44] K.S.W. Sing, Assessment of surface area by gas adsorption, in: J. Rouquerol, F. Rouquerol, P. Llewellyn, G. Maurin, K.S.W. Sing (Eds.), Adsorption by Powders and Porous Solids. Principles, Methodology and Applications, second ed., Academic Press, Oxford, 2012, pp. 237–268.
[45] P.I. Ravikovitch, A.V. Neimark, Density functional theory of adsorption in spherical cavities and pore size characterization of templated nanoporous silicas with cubic and three-dimensional hexagonal structures, Langmuir ACS J. Surf. Colloids 18 (2002) 1550–1560.
[46] S. Lowell, J.E. Shields, M.A. Thomas, M. Thommes, Characterization of Porous Solids and Powders: Surface Area, Pore Size and Density, Springer Science & Business Media, 2012.

[47] Z. Chen, Z. Luan, J. Fan, Z. Zhang, X. Peng, B. Fan, Effect of thermal treatment on the formation and transformation of Keggin Al13 and Al30 species in hydrolytic polymeric aluminum solutions, Colloids Surf. A Physicochem. Eng. Asp. 292 (2007) 110–118.
[48] C. Ye, Z. Bi, D. Wang, Formation of Al_{30} from aqueous polyaluminum chloride under high temperature: role of Al13 aggregates, Colloids Surf. A Physicochem. Eng. Asp. 436 (2013) 782–786.
[49] L. Allouche, C. Gérardin, T. Loiseau, G. Férey, F. Taulelle, Al_{30}: a giant aluminum polycation, Angew. Chem. Int. Ed. 3 (2000) 511–514.
[50] G. Fu, L.F. Nazar, A.D. Bain, Aging processes of alumina sol-gels: characterization of new aluminum polyoxycations by aluminum ^{27} NMR spectroscopy, Chem. Mater. 3 (1991) 602–610.
[51] D. Plee, F. Borg, L. Gatineau, J.J. Fripiat, High-resolution solid-state ^{27}Al and ^{29}Si nuclear magnetic resonance study of pillared clays, J. Am. Chem. Soc. 107 (1985) 2362–2369.
[52] L. Bieseki, H. Treichel, A.S. Araujo, S.B.C. Pergher, Porous materials obtained by acid treatment processing followed by pillaring of montmorillonite clays, Appl. Clay Sci. 85 (2013) 46–52.
[53] T. Zhao, W. Li, H. Wang, F. Meng, Facile synthesis of Al-pillared mesoporous montmorillonite assisted with concentrated Al_{13} solution, Chem. Res. Chin. Univ. 30 (2014) 200–204.
[54] J.-F. Lambed, S. Chevalier, R. Franck, H. Suquet, D. Barthomeuf, Al-pillared saponites. Part 2. NMR studies, J. Chemical Society Faraday Trans. 90 (1994) 675.
[55] C.A. Fyfe, G.C. Gobbi, J. Klinowski, J.M. Thomas, S. Ramdas, Resolving crystallographically distinct tetrahedral sites in silicalite and ZSM-5 by solid-state NMR, Nature 296 (1982) 530–533.
[56] M.F. Brigatti, E. Galan, B.K.G. Theng, Structures and mineralogy of clay minerals, in: F. Bergaya, G. Lagaly (Eds.), Handbook of Clay Science, second ed., Elsevier, 2013, pp. 21–82.
[57] L. Allouche, C. Huguenard, F. Taulelle, 3QMAS of three aluminum polycations: space group consistency between NMR and XRD, J. Phys. Chem. Solids 62 (2001) 1525–1531.
[58] M. Thommes, K. Kaneko, A.V. Neimark, J.P. Olivier, F. Rodriguez-Reinoso, J. Rouquerol, K.S.W. Sing, Physisorption of gases, with special reference to the evaluation of surface area and pore size distribution (IUPAC Technical Report), Pure Appl. Chem. 87 (2015).